Int. J. Heat Mass Transfer. Vol. 36, No. 12, pp. 2987–2995, 1993
Printed in Great Britain

0017–9310/93 $6.00 + 0.00

Kinetic and heat transfer-controlled solidification of highly supercooled droplets

MICHAEL EPSTEIN and HANS K. FAUSKE
Fauske & Associates, Inc., 16W070 West 83rd Street, Burr Ridge, Illinois 60521, U.S.A.

(*Received* 20 *October* 1992 *and in final form* 12 *January* 1993)

Abstract—An efficient integral profile computational method is used to solve the problem of the solidification of highly subcooled droplets. The effects of surface cooling by radiation and convection, interface crystallization kinetics and fully time-dependent heat conduction are included in the method. Particular attention is focused on the predicted drop surface temperature–time histories as these, together with available experimental luminosity–time traces for solidifying microspheres of Al_2O_3 and ZrO_2, are used to infer the coefficient of the kinetic law for Al_2O_3 crystallization—one of the crucial parameters in a recently proposed theory of underwater aluminum ignition.

INTRODUCTION

NELSON and his co-workers [1–3] have shown that pendant drops or freely falling microdrops melted by pulse heating offers an attractive method of studying the solidification of highly supercooled refractory materials. Systematic observations on the behavior of the drops, including specimens (Zr) that have reacted chemically with a component of the ambient gas mixture, reveal interesting freezing behavior. The drops are observed to remain liquid well below their equilibrium freezing points, with surface solidification commencing abruptly when some threshold (or 'critical') supercooling is attained. Owing to the release of latent heat the surface temperature (or luminosity) of the drops rises abruptly, passes through a maximum, and then falls off at a rate indicating that the internal solidification process is not complete.

Because measurements of this sort offer the possibility of inferring the crucial, but unknown kinetic parameter(s) for highly refractory metal oxide substances, Rosner and Epstein [4], initiated a theoretical study of 'nonequilibrium solidification'. The nonequilibrium theory differs from the common solidification analysis in that interface (liquid-to-solid phase) attachment kinetics is important and results in the interface temperature being lower than the fusion temperature. The Rosner–Epstein study was limited to the case of semi-infinite geometry (or, equivalently, large droplet sizes) in which the surface temperature of the drop is assumed to pass through its maximum value before the leading thermal wave is an appreciable fraction of the sphere radius. Moreover, the solidification rate laws employed in their study are valid only for low-to-moderate supercooling for which the crystallization velocity increases with increasing supercooling and, therefore, can not be used to follow the solidification event in a highly supercooled (or 'hypercooled') liquid drop. At very high supercoolings the crystallization velocity actually decreases with increasing supercooling and asymptotically approaches zero as the absolute zero of temperature is approached. Accordingly, we have extended the Rosner–Epstein [4] analysis to include both curvature effects in a spherically symmetric system and a kinetic rate law that exhibits the correct crystallization speed behavior over the entire range of possible supercoolings, from the absolute zero of temperature up to the melting point. To the best of the authors' knowledge there have been no previous theoretical treatments of combined heat-conduction- and kinetic-controlled solidification of super-cooled droplets.

KINETIC LAW OF SOLIDIFICATION (CRYSTAL GROWTH)

When the liquid/solid interface is near-planar on a microscopic scale (i.e. non dendritic) the dependence of the interface velocity v_i on the temperature T_i at the liquid/solid interface can take a number of distinct forms. Among the most important is an exponential law of the form

$$v_i = A\left(\frac{T_i}{T_{mp}}\right)\exp\left(-\frac{1.5\,T_{mp}}{T_i}\right) \times\left\{1-\exp\left[-\frac{h_{fs}M}{R_g T_{mp}}\left(\frac{T_{mp}}{T_i}-1\right)\right]\right\}. \quad (1)$$

The above expression was developed by Jackson and Chalmers [5] by considering the probability that a molecule will make a transition from solid to liquid, or liquid to solid, across the liquid/solid interface (or moving solidification front). The coefficient 1.5 in the argument of the leading exponential term in equation (1) is based on Jackson and Chalmers' [5] estimate of

NOMENCLATURE

A	crystallization wave speed parameter, equation (1)
Bi	Biot number for convective heat loss, hR/k_s
Bi_r	Biot number for radiative heat loss, $\varepsilon\sigma T_{mp}^n Rc_s/(k_s h_{fs})$
c_m, c_s	specific heats of melt and solid, respectively
h	convective heat transfer coefficient
h_{fs}	latent heat of fusion
H	dimensionless latent heat of fusion, $h_{fs}/(c_s T_{mp})$
J_1	dimensionless frozen layer heat content, $c_s/(h_{fs}R^3)\cdot\int_\xi^R r^2[T_s(r,t)-T_o]\,dr$
J_2	dimensionless melt layer heat content, $c_s/(h_{fs}R^3)\cdot\int_\delta^\xi r^2[T_m(r,t)-T_o]\,dr$
k	melt-to-solid thermal conductivity ratio, k_m/k_s
k_m, k_s	thermal conductivities of melt and solid, respectively
M	molecular weight of solidifying material
n	exponent in radiation heat-flux law, equation (6)
Q	dimensionless activation energy for solidification, $h_{fs}M/(R_g T_{mp})$
r	radial location measured from center of drop
R	radius of solidifying drop
R_g	ideal gas constant
t	time
T_c	temperature at center of drop ($r=0$)
T_i	temperature at solid/liquid interface ($r=\xi$)
T_m	temperature profile in melt region
T_{mp}	equilibrium melting point temperature
T_o	initial temperature of supercooled drop
T_s	temperature profile in solid region
T_w	temperature at surface of sphere ($r=R$)
T_∞	temperature of ambient medium
W	dimensionless crystallization wave speed parameter, AR/α_s
z	dimensionless location of solid/liquid interface (solidification front), ξ/R.

Greek symbols

α_m, α_s	thermal diffusivities of melt and solid, respectively
α	melt-to-solid thermal diffusivity ratio, α_m/α_s
β_o	drop supercooling ratio, T_o/T_{mp}
β_∞	dimensionless ambient temperature, T_∞/T_{mp}
β_∞	dimensionless ambient temperature, T_∞/T_{mp}
δ	radial location of thermal wave
Δ	dimensionless radial location of thermal wave, δ/R
ε	emittance of drop surface
θ_c	dimensionless temperature at center of drop, $c_s[T_c(t)-T_o]/h_{fs}$
θ_i	dimensionless temperature at solid/liquid interface, $c_s[T_i(t)-T_o]/h_{fs}$
$\theta_{w,max}$	maximum dimensionless temperature at surface of sphere
θ_{mp}	dimensionless equilibrium melting point, $(1-\beta_o)/H$
θ_w	dimensionless temperature at surface of sphere, $c_s[T_w(t)-T_o]/h_{fs}$
ξ	radial location of solid/liquid interface, Fig. 1
ρ	density of melt or solid
σ	Stefan–Boltzmann radiation constant
τ	dimensionless time, $\alpha_s t/R^2$
χ	temperature profile shape function for solid region (dimensionless), equation (7).

the 'transition energy' for the solidification of metals. It is assumed here that their estimate is equally valid for refractory metal oxides. Equation (1) was chosen over other proposed kinetic laws in that it provides a physical basis for estimating v_i over the entire range of possible interface temperatures T_i, from absolute zero up to the melting point. (A discussion of less complex solidification kinetic laws can be found in ref. [4].) A special application of equation (1) of interest to the authors applies to Al_2O_3 spheres (crystals) growing in Al_2O_3 melts with initial undercoolings as large as 1300 K. Note that this supercooling is much larger than what is normally possible by rapid heat loss, namely $\approx 0.2\ T_{mp}$ (Turnbull and Cech [6]), and is postulated to occur as a result of a sudden chemical transition (oxidation) from molten aluminum to metastable Al_2O_3 microdrops (Epstein and Fauske [7]). The parameter 'A' in equation (1) is related to the mobility of the liquid molecules at the solidification front. Least is known (a priori) about this 'solidification wave speed parameter' and, consequently, its numerical value for Al_2O_3 constitutes the result sought.

A careful examination of equation (1) shows that the solidification speed v_i first increases with increasing subcooling $T_{mp}-T_i$, reaches a peak value when the supercooling is sufficiently high (~ 400 K for Al_2O_3) and tends to zero at the maximum possible undercooling corresponding to a melt region at absolute zero ($T_i = 0$ K). This behavior has been observed for a select group of substances (mostly organics); however, there seems to be no strong theoretical

reason to doubt the generality of the shape of the curve produced with equation (1), (see, e.g., Knight [8]).

In terms of determining the unknown coefficient 'A' in equation (1), two alternatives present themselves. One might try to cool the liquid material rapidly enough to get into the low temperature regime where the rate of growth of the solid is very slow and a good measurement of 'A' could be obtained. Unfortunately, no one has attempted to do this with molten Al_2O_3 nor does it seem possible to cool Al_2O_3 rapidly enough to keep it in a liquid state down to the very low temperatures required (~ 100 K). It is possible, however, to obtain supercoolings of the order of several hundred degrees in rapidly cooled small molten drops. Because of the low probability of heterogeneous nucleation sites existing in the small droplets, the drops remain in the liquid state until the temperature is low enough for homogeneous nucleation to set in. This suggests the second alternative for estimating 'A', which is to exploit the experimentally observable outer surface temperature–time history of the molten oxide drop to infer the crystallization kinetic parameter 'A'. The idea is that a detailed treatment of transient directional solidification including the simultaneous effects of spherical geometry, finite crystallization kinetics, internal conduction and drop external heat loss would be able to rationalize the surface temperature–time history, thereby providing a sound basis for crystallization parameter inference. The surface luminosities of solidifying Al_2O_3 and ZrO_2 drops have been followed experimentally by Nelson *et al.* [1, 3].

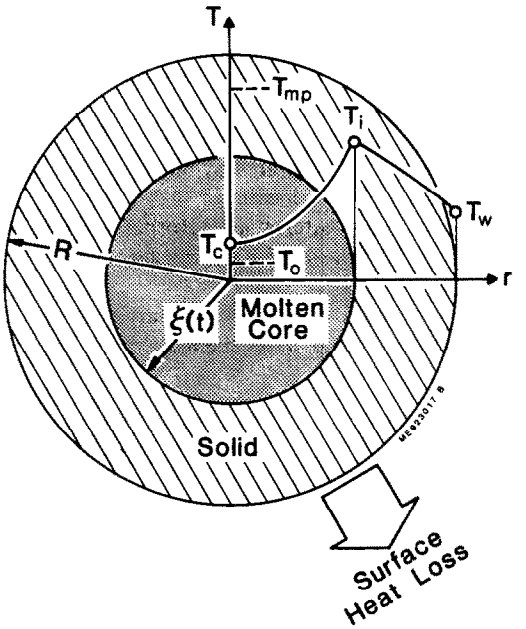

FIG. 1. Spherical wave solidification of an initially supercooled drop; illustrating temperature profile shape after thermal wave reaches drop centerline.

PHYSICAL MODEL

We consider a drop losing heat by radiation and convection at its outer surface (see Fig. 1). At time $t = 0$ a solidification front appears at the drop interface and propagates inward toward the center of the drop at a rate determined both by the conduction of heat through the annular crust and the kinetic rate of solidification given by equation (1). Since our goal is to produce a simple mathematical model of the solidification process that is compatible with available experimental observations, our study is based on the following assumptions:

(1) The drop temperature is uniform and equal to T_o at the instant of superficial solidification.

(2) The temperature field within the drop is at all times spherically symmetric, with an annular crust growing at the expense of a molten but stationary core.

(3) The solidification front is non-diffuse (sharp) on the scale of the droplet radius.

(4) Radiation transfer through a semi-transparent melt/crust is ignored and, therefore, the instantaneous heat flux from the surface of the drop is a function of instantaneous surface temperature alone.

(5) All physical properties are assumed to be constant and the density is the same for both liquid and solid.

The only serious concern relative to the assumptions stated above is whether or not during some stage of the solidifications of interest here the sharp interface assumption (number 3) breaks down. The liquid/solid interface may not be stable and may 'sprout' bumps or dendrites which will race ahead of the interface. The undercooling of the melt increases with distance from the solidification front (see Fig. 1). If the solidification velocity increases with subcooling, as is true for moderate subcoolings, then any momentary bump at the front will tend to find itself in a region of increased undercooling and therefore tend to move ahead of the rest of the solidification front, perhaps leading to a dendritic morphology. It seems doubtful that interface-kinetic parameters could be inferred when a highly non-spherical interface configuration prevails.

GOVERNING EQUATIONS

The integral profile method provides a practical and sufficiently accurate approach to the solution of phase change problems (Goodman [9]). In applying this method to the present problem reasonable functional forms for the radius dependence of the solid and liquid (melt) temperature fields, $T_s(r, t)$ and $T_m(r, t)$, are postulated, containing undetermined functions of time. The problem is closed by imposing conditions derivable from the basic partial differential equations of heat conduction for the solid and melt regions. The undetermined functions of time we introduce are a

shape function $\chi(t)$ for the temperature profile in the crust and the location of the thermal wave $\delta(t)$ or the drop centerline temperature $T_c(t)$ (after $\delta = 0$) in the melt region (see Fig. 1). We satisfy energy conservation in an average sense over the solid and liquid regions, which are separated by the liquid/solid interface at instantaneous location $r = \xi(t)$. Our integral-profile-method is pattened after Rosner and Epstein's [4] treatment of the same heat transfer problem for a semi-infinite solid.

Consideration of energy conservation at the solidification front dictates the local discontinuity of $\partial T/\partial r$:

$$\rho h_{fs}\frac{d\xi}{dt} = k_s\left(\frac{\partial T_s}{\partial r}\right)_{r=\xi} - k_m\left(\frac{\partial T_m}{\partial r}\right)_{r=\xi}. \quad (2)$$

In accord with the integral profile method, rather than demanding that $T(r, t)$ satisfy the transient heat conduction equation everywhere, we only impose the integral form of this equation:

$$\frac{d}{dt}\int_{\xi}^{R} r^2[T_s(r,t)-T_o]\,dr = \alpha_s R^2\left(\frac{\partial T_s}{\partial r}\right)_{r=R} - \alpha_s\xi^2\left(\frac{\partial T_s}{\partial r}\right)_{r=\xi} - [T_i(t)-T_o]\xi^2\frac{d\xi}{dt} \quad (3)$$

for the crust ($R \leqslant r \leqslant \xi$) and the integral form of the conduction equation:

$$\frac{d}{dt}\int_{\delta}^{\xi} r^2[T_m(r,t)-T_o]\,dr = \alpha_m\xi^2\left(\frac{\partial T_m}{\partial r}\right)_{r=\xi} - \alpha_m\delta^2\left(\frac{\partial T_m}{\partial r}\right)_{r=\delta} + [T_i(t)-T_o]\xi^2\frac{d\xi}{dt} \quad (4)$$

for the melt, where again $\delta(t)$ is the effective penetration distance of the thermal wave in the melt, at which $\partial T_m/\partial r = 0$. Beyond the time at which the thermal wave reaches the center of the drop, defined by $\delta(t) = 0$, $T_m(r, t)$ in the melt must satisfy the integral condition

$$\frac{d}{dt}\int_{0}^{\xi} r^2[T_m(r,t)-T_o]\,dr = \alpha_m\xi^2\left(\frac{\partial T_m}{\partial r}\right)_{r=\xi} + [T_i(t)-T_o]\xi^2\frac{d\xi}{dt} \quad (5)$$

together with a symmetry condition at the origin, namely $(\partial T_m/\partial r)_{r=0} = 0$. The above equations are subject to the surface heat loss condition

$$-k_s\left(\frac{\partial T_s}{\partial r}\right)_{r=R} = \varepsilon\sigma[T_w^n(t)-T_\infty^n] + h[T_w(t)-T_\infty] \quad (6)$$

where $T_w(t)$ is the temperature at the surface of the drop, i.e. $T_s(R, t)$. Equation (6) was chosen to include combined radiative and convective heat losses to the surrounding environment at temperature $T_\infty (T_o > T_\infty)$. The exponent n has its usual value of 4. However, in order to accurately model those cases for which the dominant mechanism of heat loss is radiative and $T_w \gg T_\infty$, n may be anywhere from about 2.5 to 5.0 depending on the temperature dependence of the drop-surface emittance.

The final equations governing the unknown functions $T_w(t)$, $T_i(t)$, $\xi(t)$ and either $\delta(t)$ or $T_c(t)$ are obtained by introducing reasonable temperature profiles into the integral conditions (3)–(5). The function $T_c(t)$ is the temperature at the center of the drop; it remains constant and equal to the initial temperature T_o until $\delta = 0$. After $\delta = 0$, $T_c(t)$ increases toward T_{mp}. Before $\delta = 0$ second- and third-order polynomials are assumed for the temperature-distributions in the crust and melt, respectively, and they are given by

$$\frac{T_s(r,t)-T_i(t)}{T_w(t)-T_i(t)} = \chi(t)\frac{R}{r}\left[\frac{r-\xi(t)}{R-\xi(t)}\right] + [1-\chi(t)]\frac{R}{r}\left[\frac{r-\xi(t)}{R-\xi(t)}\right]^2 \quad (7)$$

$$\frac{T_m(r,t)-T_o}{T_i(t)-T_o} = \frac{\xi(t)}{r}\left[\frac{r-\delta(t)}{\xi-\delta(t)}\right]^3. \quad (8)$$

After $\delta = 0$ a second order polynomial is assumed for the melt:

$$\frac{T_m(r,t)-T_c(t)}{T_i(t)-T_c(t)} = \left[\frac{r}{\xi(t)}\right]^2. \quad (9)$$

Note that the above profiles have the desirable property of temperature continuity at the solidification front [$r = \xi(t)$], and the desirable property of melt temperature profile compatibility at the instant $\delta(t) = 0$. Moreover, in writing equations (8) and (9) we have already satisfied the conditions $\partial T_m/\partial r = 0$ at $r = \delta(t)$ before $\delta = 0$ and $\partial T_m/\partial r = 0$ at $r = 0$ after $\delta = 0$. The temperature profile proposed for the crust, equation (7), contains a shape function $\chi(t)$ which must be determined as part of the solution.

From equations (1), (2)–(4), and (6)–(8) the following system of dimensionless equations is obtained for purposes of numerical computation during the time span before $\delta = 0$ (see Nomenclature list for meanings of symbols):

$$\frac{dz}{d\tau} = -\frac{(\theta_i-\theta_w)\chi}{z(1-z)} - k\theta_i\left(\frac{3}{z-\Delta}-\frac{1}{z}\right) \quad (10)$$

$$\frac{dJ_1}{d\tau} = -(\theta_i-\theta_w)(1-\chi)\left(\frac{1+z}{1-z}\right) - \theta_i z^2\frac{dz}{d\tau} \quad (11)$$

$$\frac{dJ_2}{d\tau} = \alpha z^2\theta_i\left(\frac{3}{z-\Delta}-\frac{1}{z}\right) + \theta_i z^2\frac{dz}{d\tau} \quad (12)$$

$$\frac{dz}{d\tau} = -W(\beta_o+H\theta_i)\exp\left(-\frac{1.5}{\beta_o+H\theta_i}\right)$$

$$\cdot\left[1-\exp\left(Q-\frac{Q}{\beta_o+H\theta_i}\right)\right] \quad (13)$$

$$(\theta_i-\theta_w)\left(\frac{1+z-\chi}{1-z}\right)=Bi_r[(\beta_o+H\theta_w)^n-\beta_\infty^n]$$

$$+\frac{Bi}{H}(\beta_o-\beta_\infty+H\theta_w) \quad (14)$$

$$J_1=\tfrac{1}{3}\theta_i(1-z^3)$$

$$-\tfrac{1}{12}(\theta_i-\theta_w)(1-z)[\chi(1+z)+3+z] \quad (15)$$

$$J_2=\theta_i z(z-\Delta)[\tfrac{1}{4}z-\tfrac{1}{20}(z-\Delta)]. \quad (16)$$

As soon as δ reaches $r=0$, it becomes necessary to include the boundary condition $\partial T_m/\partial r=0$ at $r=0$ and, therefore, to consider the global heat balance for the melt given by equation (5) and the corresponding temperature profile given by equation (9). Thus for the period after $\delta=0$ we replace equations (10), (12) and (16) by

$$\frac{dz}{d\tau}=-\frac{(\theta_i-\theta_w)\chi}{z(1-z)}-\frac{2k}{z}(\theta_i-\theta_c) \quad (17)$$

$$\frac{dJ_2}{d\tau}=2\alpha z(\theta_i-\theta_c)+\theta_i z^2\frac{dz}{d\tau} \quad (18)$$

$$J_2=\tfrac{1}{5}z^3(\theta_i-\theta_c)+\tfrac{1}{3}\theta_c z^3. \quad (19)$$

The solutions of equations (10)–(16) must satisfy the initial conditions $z=\Delta=1$, $J_1=J_2=\theta_w=\theta_i=0$ at $\tau=0$. In order to provide useful starting values in a forward numerical integration scheme for this coupled system of equations, small-time power series solutions of the form

$$\sum_{m=0}^{\infty}a_m\tau^{m/2}$$

were obtained. In addition, to utilize available computer subroutines, equations (10)–(19) were converted to an equivalent coupled system of first-order ordinary differential equations. This somewhat tedious algebraic operation included equating the conduction-heat-flux jump condition, equation (10) before $\delta=0$ or equation (17) after $\delta=0$, with the kinetic rate equation, equation (13), to obtain an explicit differential equation where $dz/d\tau$ has been eliminated in favor of the other dependent variables. Numerical integration was performed using a forward integration procedure based on the Gear [10] method (see also Hindmarsh [11]).

PARAMETER SELECTION, NUMERICAL RESULTS AND KINETIC WAVE SPEED PARAMETER FOR PENDANT DROPS OF AL_2O_3

Within the framework of the present model, drop solidification behavior depends on nine parameters; namely, Bi_r, Bi, Q, H, W, β_o, β_∞, α, and k. Since little thermal conductivity data exists for subcooled molten refractory metal oxides, such as Al_2O_3, the solid-to-liquid thermal diffusivity and thermal conductivity ratios are assumed to be unity ($\alpha=k=1.0$). It can be shown from nucleation theory (Chalmers [12]) that in the absence of foreign nucleation sites or vibration the supercooling in a melt is practically independent of cooling rate and approximately equal to 0.2 T_{mp}. Thus for an environment where molten microdrops cool largely undisturbed the appropriate value of the parameter β_o is 0.8. Little is known about the solidification wave speed parameter W and, as already mentioned, this is the parameter we desire to infer from laboratory data.

The values of the remaining five parameters, namely Bi_r, Bi, Q, H, β_∞, are dictated by available drop solidification data. In particular we consider the situation studied by Nelson *et al.* [3] where a 2 mm-diameter, laser-melted Al_2O_3 pendant droplet cooled and solidified in a 0.35 m s^{-1} flow of oxygen gas. During the course of the experiment the pendant drop was suspended from a single crystal sapphire rod. The drop surface luminosity was followed experimentally and the luminosity trace is depicted in Fig. 2. After the laser was turned off the luminosity trace shows a smooth cooling curve for about 0.15 s, a sudden increase for about 21 ms followed by a relatively constant segment for about 0.6 s. The sudden increase in luminosity is believed to correspond to the release of latent heat from a solidification wave propagating into the supercooled drop. This brightening effect is referred to in the literature as the 'spearpoint' because of the spear-like profile observed on time exposed photographs of cooling metal droplets ('sparks'). The final flat portion of the luminosity trace is believed to be the result of a balance between the heat loss at the surface and the latent heat generated within the drop as the solidification process continues. Note that there is a difficulty of accurately locating the termination of solidification ($\xi=0$ 'event') on the luminosity trace. For this reason, and because the present model indicates that the drop freezing time is rather insensitive to the solidification wave speed W for moderate-to-high values of W, freezing-time predictions are not particularly useful for inferring crystallization kinetics.† However, the luminosity rise time that defines the duration of the brightening event on the luminosity trace could possibly be used for this purpose, depending on the validity of the model described in the foregoing.

Applying the Ranz and Marshall correlation (see, e.g., Bird *et al.* [13]) for forced convection heat trans-

† Freezing time predictions may be useful for inferring kinetic parameters if hypercooled droplet states, defined by the inequality $c_m(T_{mp}-T_o)>h_{fs}$, can be achieved. These predictions are beyond the scope of the present paper.

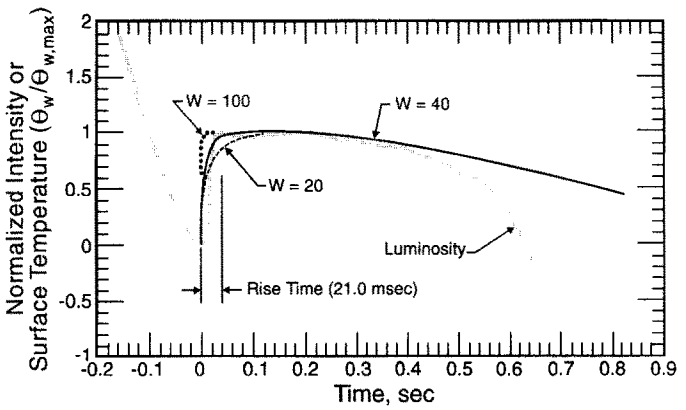

FIG. 2. Comparison of normalized luminosity-time trace with predicted normalized drop surface time histories for wave speeds $W = 20, 40, 100$. Trace for 2 mm-diameter Al_2O_3 pendant drop from Nelson *et al.* [3].

fer from a single sphere, the heat transfer coefficient for the Al_2O_3 pendant drop in flowing oxygen is estimated to be $h = 127.0\ W\ m^{-2}\ K^{-1}$. This estimate was obtained by assuming a gas film temperature of 1200 K at which the viscosity, thermal conductivity and heat capacity of oxygen are 5.52×10^{-5} kg m^{-1} s^{-1}, 0.085 W m^{-1} K^{-1}, and 1.12×10^3 J kg^{-1} K^{-1}, respectively. The thermal conductivity of solid Al_2O_3 is about $k_s = 7.5\ W\ m^{-1}\ K^{-1}$ (Wood and Deem [14]). Inserting these estimates into the definition of the 'convective Biot number' gives $Bi = 0.017$. The value of the 'radiation Biot number' could be obtained if the total emissivity ε of the Al_2O_3 drop surface is known. The available data indicates an Al_2O_3 emissivity of about 0.26 at a surface temperature of 1100 K (see e.g., Hottel and Sarofim [15]). Using this value our predicted solidification period is much longer than indicated by the luminosity trace shown in Fig. 2. If ε is taken to be nearly unity, then the present theory predicts total drop solidification at about 0.8 s which compares favorably with the observed value of ≈ 0.5 s (see below). We tentatively conclude that the effective emissivity of high-temperature Al_2O_3 (~ 2000 K) is nearly unity. The correctness of this conclusion must, of course, await the results of future high-temperature measurements of ε for Al_2O_3. Note that the difference between the predicted and observed solidification times is not due to kinetics, as the drop solidification time is rather insensitive to the pre-exponential constant 'A' (or, equivalently W) for values of 'A' that are large enough to yield a surface brightening segment on the predicted drop cooling curve. Using $\varepsilon = 1$, we estimate a radiation Biot number of $Bi_r = 0.26$ for the freezing Al_2O_3 drop studied by Nelson *et al.* [3]. The values of the other pertinent parameters are $H = 0.36$, $Q = 6.1$, $\beta_o = 0.8$, and $\beta_\infty = 0.13$. These dimensionless numbers were evaluated by inserting the following additional Al_2O_3 property values: $c_s = 1.39 \times 10^3$ J kg^{-1} K^{-1} (Stull and Prophet [16]), $\rho = 3.8 \times 10^3$ kg m^{-3}, and $h_{fs} = 1.16 \times 10^6$ J kg^{-1} (Samsonov [17]).

Typical results of the numerical solutions are shown in Figs. 3, 4, and 5 for wave speed parameters $W = 2$, 100, and 1000, respectively. The dimensionless parameters used to generate these figures pertain to the experimental conditions investigated by Nelson *et al.* [3] and discussed in the foregoing. The solutions exhibited in Fig. 3 correspond to the case of very sluggish solidification kinetics (low W). In this limit surface heat losses dominate over the latent heat release rate within the drop and the solid/liquid interface temperature remains well below the equilibrium melting temperature. Different behavior is observed in Fig. 4 for rapid interface kinetics ($W = 100$). The solidification rate starts out at the kinetic rate dictated by equation (1) (or, equivalently, equation (13)), then decelerates, as indicated by the kink in the $z(\tau)$ curve about when the temperature at the drop center, θ_c, starts rising. At a dimensionless time near $\tau = 0.2$ (in the present case) the molten core has been raised essentially to the melting point [$\theta_{mp} = (1-\beta_o)/H$], and further heat rejection must occur solely through

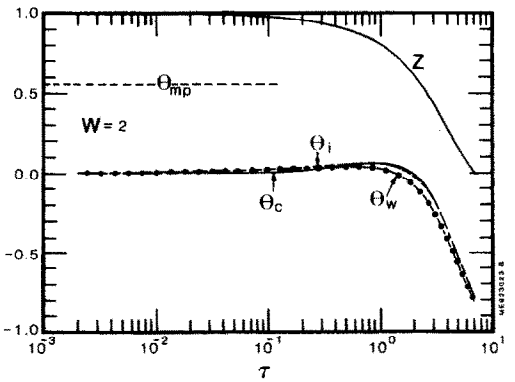

FIG. 3. Time histories (dimensionless) of drop surface temperature, θ_w, solidification front temperature, θ_i, drop centerline temperature, θ_c, and solidification front location, z, for sluggish crystallization kinetics. Results for Al_2O_3 properties and experimental conditions of Nelson *et al.* [3]; $H = 0.36$, $Q = 6.1$, $\beta_o = 0.8$, $\beta_\infty = 0.13$, $Bi = 0.017$, $Bi_r = 0.26$, $n = 4.0$.

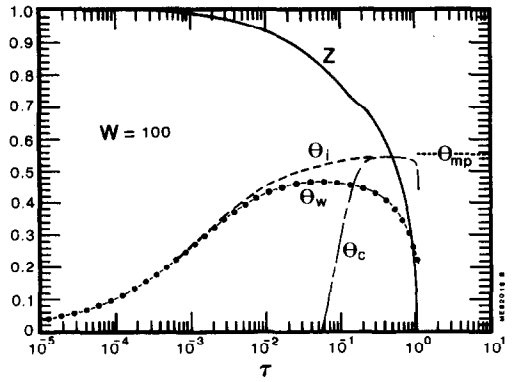

FIG. 4. Time histories (dimensionless) of drop surface temperature, θ_w, solidification front temperature, θ_i, drop centerline temperature, θ_c, and solidification front location, z, for rapid crystallization kinetics. Results for Al_2O_3 properties and experimental conditions of Nelson *et al.* [3]; $H = 0.36$, $Q = 6.1$, $\beta_o = 0.8$, $\beta_\infty = 0.13$, $Bi = 0.017$, $Bi_r = 0.26$, $n = 4.0$.

the annular crust. The temperature at the solidification front rises rapidly from the initial drop temperature ($\theta_i = 0$) to the melting point and ultimately merges with the drop centerline temperature at $\tau \approx 0.2$. While the wave temperature is at or nearly equal to the equilibrium melting point the wave speed is conduction-heat-transfer limited. Interestingly enough, just before the freezing process is complete, both the solidification wave temperature and the drop center temperature fall below the melting point and the shrinking molten core returns to the subcooled condition. This occurs because near the completion of the solidification process the conduction-limited freezing rate tends to propagate more rapidly than is permitted by solidification kinetics. In the very rapid phase change kinetics regime (Fig. 5 for $W = 1000$) the time to 'heat' the solidification front to the equilibrium melting point T_{mp} is so small that for all practical purposes the front is at all times at T_{mp} and the freezing rate of the droplet is exclusively heat-transfer controlled.

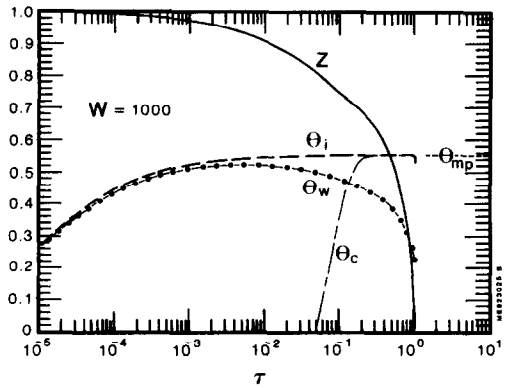

FIG. 5. Time histories (dimensionless) of drop surface temperature, θ_w, solidification front temperature, θ_i, drop centerline temperature, θ_c, and solidification front location, z, for very rapid crystallization kinetics. Results for Al_2O_3 properties and experimental conditions of Nelson *et al.* [3]; $H = 0.36$, $Q = 6.1$, $\beta_o = 0.8$, $\beta_\infty = 0.13$, $Bi = 0.017$, $Bi_r = 0.26$, $n = 4.0$.

Note that after the interface temperature and the drop centerline temperature coincide the temperature gradient in the molten core disappears and conditions are no longer favorable to dendritic growth (in pure materials). Clearly, early in the solidification process the temperature gradient in the melt is very large and the solid/liquid interface is unstable. However, the rate of kinetic solidification is so rapid during this period that dendrites may not have time to form.

We note from Figs. 4 and 5 that the drop surface temperature θ_w passes through a maximum value $\theta_{w,max}$ when the solidification wave temperature is still below the equilibrium melting point θ_{mp}. Unfortunately, the surface luminosity trace for Al_2O_3 (Fig. 2) only gives pyrometer readings (in arbitrary units) and therefore does not permit comparisons with the predicted $\theta_{w,max}$ to infer the wave speed parameter W. However, the rise time on the luminosity trace can be used to estimate W. In particular, we seek to determine the value of W that brings the predicted time it takes for the surface temperature to rise to its maximum value into coincidence with the observed duration of the brightening segment on the luminosity trace of about 21.0 ms. There is a certain degree of arbitrariness in applying this approach in that the predicted surface temperature history $\theta_w(\tau)$ shows a very broad maximum (see Figs. 4 and 5), making it difficult to identify a specific theoretical surface temperature rise-time for comparison with the rise time on the luminosity trace.

We proceed by inquiring whether there exists a choice of W for input into the model which is able to approximately reproduce the observed rise time and the very gradual attenuation that follows the abrupt rise on the luminosity trace. The best fit is obtained with $W = 40$, although one could argue that W's as large as 60 and as small as 30 are also able to reconcile the luminosity trace. However, when W falls outside this range the model does not satisfactorily predict the observed brightening time. The comparison of the model for $W = 40$ with the luminosity trace is shown in Fig. 2. Also shown in the figure is the early $\theta_w(\tau)$ behavior for the numerical cases $W = 20$, 100. In this figure the luminosity trace is normalized so that the brightness is zero at the onset of solidification and the maximum brightness along the plateau is taken to be unity. The predicted surface temperature $\theta_w(\tau)$ is normalized with respect $\theta_{w,max}$ so that it also only takes on values between zero and unity.

Note that it is not meaningful to compare the function $\theta_w(\tau)$ with the shape of the luminosity trace in regions where the luminosity is changing, as the relation between light intensity and temperature is highly nonlinear. All we can determine from the luminosity trace is the time to maximum luminosity and the duration of the subsequent period in which a

slow decrease in brightness (or surface temperature) occurs. In this connection we observe from Fig. 2 that the model predicts that drop solidification is complete at about 0.8 s, while the luminosity trace indicates that the actual time at which solidification ceases is roughly 0.5 s. This level of agreement should be regarded as reasonable for problems of this type, especially in view of current physical property uncertainties for supercooled Al_2O_3, the possibility of the transition from planar to dentritic growth early in the solidification transient and the fact that the pendant drops do not form perfect spheres as assumed in the model. It is also worth noting that the predicted dimensionless thermal wave location at the end of the period of rapid temperature rise (i.e. at $t \approx 21$ ms in Fig. 2) is $\Delta = \delta/R = 0.37$. Thus for the experimentally interesting case treated above, thermal wave penetration is an appreciable fraction of the sphere radius and is large enough to justify the present model which accounts for curvature effects in a spherically symmetric system.

To convert the dimensionless inference $W = 40$ to the physical crystallization wave speed parameter 'A', we insert the property value estimates for solid Al_2O_3 and the pendant drop radius $R = 10^{-3}$ m into the relation (definition) $A = \alpha_s W/R$ to obtain $A = 5.72 \times 10^{-2}$ m s^{-1}.

KINETIC WAVE SPEED PARAMETER FOR FREELY FALLING DROPS OF ZrO_2 AND AL_2O_3

Quantitative information about the luminosity–time behavior of solidifying ZrO_2 droplets produced by the combustion of freely falling molten Zr spheres in oxygen/gas mixtures has been reported by Nelson *et al.* [1]. (The chemical conversion of Zr to ZrO_2 was complete before the onset of ZrO_2 solidification.) They converted the pyrometry readings to drop temperatures and the estimated drop-temperature ranges immediately before and after solidification are shown by the shaded regions in Fig. 6. Note that the rapid rise in drop temperature due to the onset of solidification occurs in about 0.05 ms. Recall that the luminosity rise time for the pendant drop of Al_2O_3 was much longer and approximately equal to 21.0 ms.

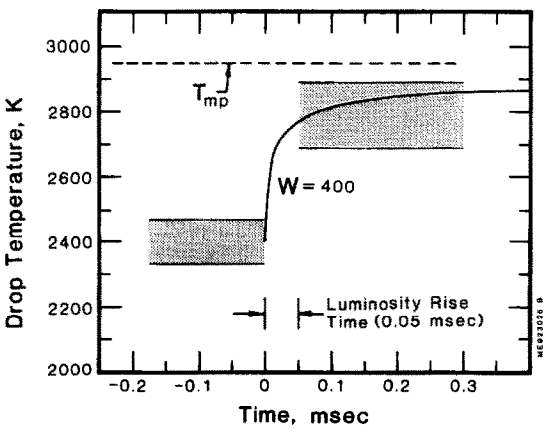

FIG. 6. Predicted surface temperature-time history for freely falling and solidifying 5.26 μm-diameter ZrO_2 drop; comparison with measured drop temperature uncertainty band (Nelson *et al.* [1]).

It is of interest to use the present model to infer the crystallization wave speed parameter for ZrO_2. The physical property values $k_s = 2.5$ W m^{-1} K^{-1} (Wood and Deem [14]), $c_s = 650.0$ J kg^{-1} K^{-1} (Stull and Prophet [16]), $\rho = 5.4 \times 10^3$ kg m^{-3}, $h_{fs} = 7.1 \times 10^5$ J kg^{-1} (Samsonov [17]), $\varepsilon = 1.0$, and $T_{mp} = 2950$ K for ZrO_2; together with the experimental conditions $T_o = 2400 \pm 70$ K and $R = 2.63 \times 10^{-4}$ m satisfy all the model input requirements once the selection of W is made. Note that the dominant mode of heat loss for this case is radiation. Thus we assume $n = 4$ and $h = 0$ (or $Bi = 0$). Figure 6 presents the surface temperature–time history result of the computer solution for $W = 400$. After making a number of computer runs for various values of W, this value (± 100) was selected as the most reasonable choice in that the corresponding predicted temperature falls within the measured drop-temperature uncertainty band and most of the predicted temperature increase occurs during the observed luminosity rise period. The physical value of the kinetic wave speed parameter for ZrO_2 is, then, $A = 1.1$ m s^{-1}. This is noticeably above the inferred kinetic wave speed parameter for Al_2O_3. Thus it would appear that kinetic limitations to solidification in Al_2O_3 are considerably more likely than in ZrO_2.

There is one additional study by Nelson *et al.* [2] that should be mentioned here. Luminosity traces were obtained for laser-melted Al_2O_3 drops shaken from the single crystal sapphire rod mentioned previously and allowed to cool while falling freely in air. While the reported luminosity trace is too coarse to allow determination of the luminosity rise time as the heat of solidification is released, it is clear from the trace that the rise is rapid on a 10 ms time scale. It is possible, then, that under free-fall conditions the crystallization wave speed parameter for Al_2O_3 is of the order of that inferred for ZrO_2 under similar free fall cooling conditions. If this is the case it certainly remains to be seen why sluggish kinetic rates dominate the superficial solidification of supercooled pendant drops and comparatively rapid interface kinetics initiate the solidification process within supercooled droplets in free fall. In view of this uncertainty, it seems necessary at present to assume that the kinetic wave speed parameter of the Jackson–Chalmers [5] rate law for Al_2O_3 ranges from the low value inferred for pendant metal oxide drops up to the relatively high value inferred for freely falling ZrO_2 drops and, therefore, that 'A' for Al_2O_3 falls within the interval 0.057–1.1 m s^{-1}.

ACCURACY OF THE INTEGRAL-PROFILE METHOD

To gain confidence in the numerical results it is prudent to consider the accuracy of the integral

method by comparison with closely related exact (numerical) solutions. Of course, these exact solutions pertain to much less general problems than the one treated here. There is no need to check the accuracy of the integral method in the limit of simple kinetic control. If W is sufficiently small the temperature profiles in the annular crust and molten core of the droplet are uniform throughout most of the solidification process, i.e. $\theta_i \approx \theta_c \approx \theta_w$ (see Fig. 3). In this limit of kinetically controlled solidification the differential equation for the drop temperature becomes

$$\frac{1}{3}\frac{d\theta_i}{d\tau} = -Bi_r[(\beta_o + H\theta_i)^n - \beta_\infty^n] + \frac{Bi}{H}(\beta_o - \beta_\infty + H\theta_w) - z^2\frac{dz}{d\tau} \quad (20)$$

which, when combined with equation (13) for the kinetic rate of solidification, is all that is necessary to predict the drop temperature and solidification front location. The validity of this equation is now independent of our profile method—and hence exact within the framework of our physical model. In terms of comparing the integral method with available solutions, it follows that the regime of conduction-limited solidification ($W \to \infty$) constitutes the most stringent test of accuracy of the method.

Goodling and Khader [18] and Tao [19] numerically solved the problem of freezing a saturated liquid ($\beta_o = 1.0$) inside a sphere cooling by convection. They reported the time it would take to completely freeze a drop in the limit of conduction control ($W \to \infty$) and for Biot numbers $0.1 \leqslant Bi \leqslant 10.0$ and dimensionless latent heats $0.1 \leqslant H \leqslant 7.5$. The present method was found to faithfully reproduce their numerical results for the dependence of the solidification time on Bi and H to within an accuracy of 14%. For physically realistic values of H in the range 0.1–0.75, the results were especially encouraging, with the integral method representing the exact numerical solutions to better than 8%.

CONCLUSIONS

Using an integral method we have studied the combined effects of interface solidification kinetics and heat conduction on the solidification rates within highly supercooled refractory material drops losing heat by surface radiation and convection. By comparing the predicted drop surface temperature–time histories with the important features of available luminosity–time records for solidifying Al_2O_3 and ZrO_2 drops we were able to infer the numerical values of the crystallization velocity coefficient for these materials in the Jackson–Chalmers [5] rate law. These inferences may be important to developing an understanding of underwater aluminum ignition as it is has been postulated that Al_2O_3 crystal growth represents the barrier to chemical energy releases during an aluminum/water physical explosion (Epstein and Fauske [7]).

REFERENCES

1. L. S. Nelson, H. S. Levine, D. E. Rosner and D. E. Kurzius, The combustion of zirconium drops in oxygen/rare gas mixtures, *High Temp. Sci.* **2,** 343–375 (1970).
2. L. S. Nelson, M. Blander, S. R. Skaggs and K. Keil, Use of a CO_2 laser to prepare chondrule-like spherules from supercooled molten oxide and silicate droplets, *Earth and Planetary Science Letters* **14,** 338–344 (1972).
3. L. S. Nelson, N. L. Richardson, K. Keil and S. R. Skaggs, Effects of oxygen and argon atmospheres on pendant drops of aluminum oxide melted with carbon dioxide laser radiation, *High Temp. Sci.* **5,** 138–154 (1973).
4. D. E. Rosner and M. Epstein, Simultaneous kinetic and heat transfer limitations in the crystallization of highly undercooled melts, *Chem. Engng Sci.* **30,** 511–520 (1975).
5. K. A. Jackson and B. Chalmers, Kinetics of solidification, *Canadian J. Phys.* **34,** 473–490 (1956).
6. D. Turnbull and R. E. Cech, Microscopic observation of the solidification of small metal droplets, *J. Appl. Phys.* **21,** 804–810 (1950).
7. M. Epstein and H. K. Fauske, A crystallization theory of underwater aluminum ignition, *Proceedings of the 5th International Topical Meeting on Reactor Thermal Hydraulics*, Vol. II. pp. 637–645. Salt Lake City (1992).
8. C. A. Knight, *The Freezing of Supercooled Liquids.* Van Nostrand, Princeton, New Jersey (1976).
9. T. R. Goodman, The heat-balance integral and its application to problems involving a change of phase, *Trans. ASME* **80,** 335–342 (1958).
10. C. W. Gear, *Numerical Initial Value Problems in Ordinary Differential Equations.* Prentice Hall, Englewood Cliffs, New Jersey (1971).
11. A. C. Hindmarsh, GEAR: Ordinary differential equation system solver, UCID-30001, Rev. 3, Lawrence Livermore National Laboratory (Dec. 1972).
12. B. Chalmers, *Principles of Solidification.* Wiley, New York (1964).
13. B. R. Bird, W. E. Stewart and E. L. Lightfoot, *Transport Phenomena.* Wiley, New York (1960).
14. W. D. Wood and H. W. Deem, Thermal properties of high temperature materials, RSIC-202, Battelle Memorial Institute (June 1964).
15. H. C. Hottel and A. F. Sarofim, *Radiative Transfer.* McGraw-Hill, New York (1967).
16. D. R. Stull and H. Prophet, *JANAF Thermochemical Tables* (2nd Edn). National Bureau Standards-37 (1971).
17. G. V. Samsonov, *The Oxide Handbook.* IF/Plenum (1973).
18. J. S. Goodling and M. S. Khader, Inward solidification with radiation-convection boundary condition, *J. Heat Transfer* **96,** 114–115 (1974).
19. L. C. Tao, Generalized numerical solutions of freezing a saturated liquid in cylinders and spheres, *A.I.Ch.E. Jl* **13,** 165–169 (1967).